Indian Journal of Geo Marine Sciences
Vol. 48 (04), April 2019, pp. 566-575

Sensitivity of a Red Sea numerical wave model to spatial and temporal resolution of forcing wind field

Khalid M. Zubier* & Sameer H. Gharbi

Marine Physics Department, Faculty of Marine Sciences, King Abdulaziz University,
Jeddah, Saudi Arabia
*[E-mail: kzubier@kau.edu.sa]

Received 23 August 2017; 09 January 2018

Simulating waves using numerical wave models provide essential wave information for navigational safety and coastal protection applications. Accuracy of such simulations depends mainly on the accuracy of the forcing wind fields, which are influenced by the wind fields' spatial and temporal resolutions. In this study, the sensitivity of a SWAN-based Red Sea wave model to spatial and temporal resolutions of forcing wind fields was investigated. The sensitivity analysis showed that forcing the wave model with wind fields of low spatial and/or temporal resolutions will affect the quality of wave model outputs, not only in terms of integrated wave parameters, but also in terms of the overall wave energy distribution in both frequency and directional domains. This study suggests that the spatial resolution of the forcing wind filed plays more significant role than the temporal resolution on the quality of the wave model predictions.

[Keywords: Red Sea; Ocean waves; Atmospheric model; Global forecasting system; Wave model; Simulating waves near shore]

Introduction

In coastal areas as well as open seas, wind-generated waves represent one of the most energetic dynamical processes. Accurate short- and long-term wave information are essential for both navigational safety and coastal protection. Spatially-limited long-term wave observations obtained through conventional methods (gauges, buoys, riders, etc.) are utilized in producing wave climatology for specific locations. Satellite-based wave observations have more spatial coverage; however, they are temporally-limited due to time span between repeated satellite tracks. Both conventional and satellite-based wave observations are used in the validation/verification procedures of numerical wave models that represent the most efficient and cost-effective tools to simulate wave conditions in both open seas and coastal areas.

Accuracy of numerical wave models in simulating wave conditions depends mainly on the quality and the resolution of the forcing wind fields[1-12]. The higher the temporal and spatial resolutions of the forcing wind filed the more the ability to capture wind and wave variability in both time and space. Forcing wind fields are typically obtained from operational atmospheric models that provide predicted wind fields on global or regional scales. These predicted wind fields are made available online by several sources (e.g. Mesoscale Meteorological Model (MM5), Weather Research and Forecasting (WRF), European Centre for Medium-Range Weather Forecasts (ECMWF), Global Forecasting System (GFS) and Navy Operational Global Atmospheric Prediction System (NOGAPAS)) for use by public and research communities. Such wind fields can be downloaded from relevant sources, either as unprocessed (raw) or processed (analyzed) predictions, with a wide range of spatial and temporal resolutions. Bathymetry also represents another input to the numerical wave models and its quality and resolution significantly influence the accuracy of the numerical wave model outputs specially for simulating wave conditions in shallow water areas.

The Red Sea (Fig. 1) is a long narrow basin separating Africa from Asia, extending from SSE to NNW between latitudes 12° 30' N and 30° N, along an almost straight line with a total length of 1932 km and average width of 280 km. In general, climate of the Red Sea is strongly affected by the north-east and southwest monsoon system over the Indian Ocean. Based on wind patterns, the Red Sea can generally be divided into three main regions: Northern, Southern and Intermediate[13-16]. In the northern region (Northward of Latitude 20° N), the prevailing winds are mainly NNW all year round. The southern region

(Southward of Latitude 18° N) is subject to two annually changing monsoonal events: during the NE monsoon (October to May) winds blow into the Red Sea from the SSE, while during the SW monsoon (June to September) winds over the southern Red Sea are from the NNW. Intermediate region (Latitudes between 18° and 20° N) develops only in the winter months and it varies temporally in size and oscillates in position during this period. Despite the fact that such wind patterns can generate energetic wave conditions, the Red Sea is extremely lacking in terms of conventional wave measurements. However, several studies have been carried out to simulate wave conditions in the Red Sea using numerical wave modeling[17-28]. Spatially-limited conventional wave measurements and/or temporally-limited satellite wave observations were used in these studies for model validation/verification purposes. These studies have shown good performances of numerical models in simulating the observed significant wave heights and to lesser extent in simulating the peak wave periods. Nevertheless, some of these studies have indicated the importance of the quality and resolutions of forcing wind fields to account for the effects associated with local unusual wind patterns and complex orography.

SWAN (acronym for Simulating WAves Nearshore) is a numerical wave model that has been originally developed to simulate wave in the near-shore areas[29]; however, further developments in the model allowed its application to areas as large as marginal seas[30-32]. Since its first release by Delft University of Technology (Netherlands), this model has been receiving continuous upgrading to account for mechanisms additions and improvements. This model is becoming widely used for simulating wave conditions in hindcasting and forecasting modes at areas with different spatial oceanic scales[33-42].

In this study, the sensitivity of a SWAN-based Red Sea wave model to the spatial and temporal resolutions of the forcing wind filed is fully investigated.

Materials and Methods

Forcing wind field

Predicted wind fields over the Red Sea were obtained from GFS which is a global numerical weather prediction model that is operationally run by the National Oceanic and Atmospheric Administration (NOAA). GFS provide re-analyzed wind fields at different spatial and temporal resolutions; however, the wind field with highest resolutions (GFS4_anl) has been utilized in this study. From the original GFS4_anl wind filed with temporal resolution of 3 hrs and spatial resolution of 0.5° x 0.5° (THHD), three additional sub-sampled wind fields were generated (THOD, SHHD and SHOD) for which resolution details are given in Table 1. These wind fields cover the period from 20 February to 01 May 2010, which constitute the study period.

KAUST buoy Data

In correspondence to the study period, hourly wind (speeds and directions) and wave (significant wave

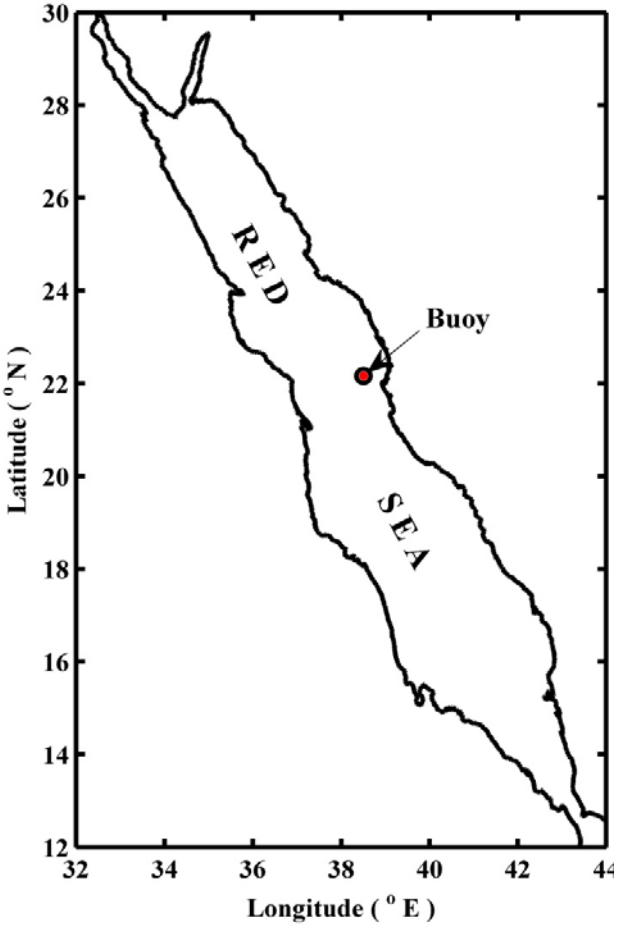

Fig. 1 — Red Sea map showing buoy location.

Table 1 — Temporal and spatial resolutions of different forcing wind fields.

Forcing Wind Filed	Temporal Resolution	Spatial Resolution
THHD	3 Hours	0.5° X 0.5°
THOD	3 Hours	1 ° X 1 °
SHHD	6 Hours	0.5° X 0.5°
SHOD	6 Hours	1 ° X 1 °

heights, peak and mean wave periods) observations made at KAUST Station (22.162° N 38.500° E) were obtained from King Abdullah University of Science and Technology (KAUST) for the study period (Fig. 1). These buoy observations are also available at the National Data Buoy Center (NDBC) web site (Station 23020).

ENVISAT data

Satellite-based wind and wave data corresponding to the study period and obtained by the Environmental Satellite (ENVISAT), have been requested from Technical University of Delft using web-based Radar Altimeter Data Acquisition Service (RADS). Figure 2 shows ENVISAT tracks over the Red Sea during the study period, including two cycles (87 and 88) and 20 tracks. The spatial and temporal resolutions along the tracks are 7.5 km and 1.114 sec, respectively.

Bathymetric data

Gridded bathymetric data set for the study area (Red Sea) was obtained from General Bathymetric Chart of the Oceans (GEBCO) website. The 'GEBCO_2014 Grid' that was utilized in this study represent a 30 arc-second interval grid generated from compilation grids of measured bathymetry from number of sources.

SWAN wave model

In this study, the numerical wave model SWAN was used to simulate the waves in the Red Sea for the study period. This third-generation spectral wave model is based on the following action balance equation:

$$\frac{\partial}{\partial t} N + \frac{\partial}{\partial x} C_x N + \frac{\partial}{\partial y} C_y N + \frac{\partial}{\partial \sigma} C_\sigma N + \frac{\partial}{\partial \theta} C_\theta N \frac{S}{\sigma} \quad \ldots (1)$$

where N is wave action density, equal to energy density divided by relative frequency ($N = E/\sigma$), (x,y) are spatial variables, (t) is time and (σ,θ) are the relative wave frequency and direction of wave propagating, respectively. The term C with respective subscript represents the propagation velocities in x, y, σ and θ spaces. The first term on the left hand side of Equation (1) represents the rate of change of action in time and the second and the third terms represent the propagation of action in the (x,y) space. The fourth and fifth terms represent, respectively, the frequency shift and refraction induced by depth and currents. In the right-hand side of Equation (1), the source and sinks term (S) represents the effects of generation, dissipations and nonlinear wave-wave interactions. Since wave-current interaction is beyond the scope of this study, the developed SWAN-based Red Sea wave model is based on the energy balance version of Equation (1), with the modeling scheme given in Table 2.

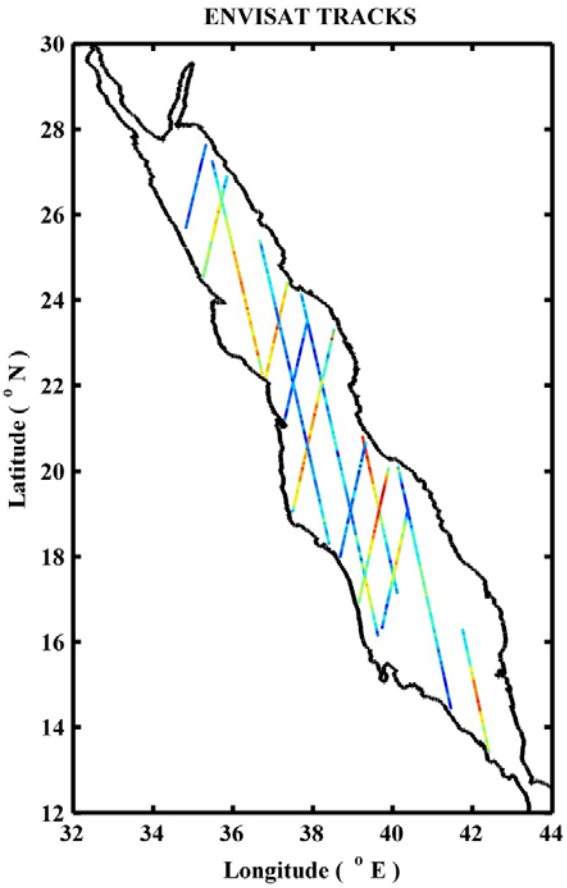

Fig. 2 — ENVISAT tracks over the Red Sea during study period with some tracks repeated. A long-track color gradient indicates wave height variation from high (red) to low (blue) and not for scale.

Table 2 — Modeling scheme of developed SWAN-based Red Sea wave model.

Coordinates	Spherical
Grid Size	0.1° x 0.1°
Directional Range	Full Circle (360°)
Number of Directions	72
Frequency Range	0.04 – 0.6 s^{-1}
Number of Frequencies	24
Wind Growth Formulation	Janssen (1989,1991)
Whitecapping	Janssen (1990)
Quad. Interactions	ON
Breaking	ON
Friction	ON

Statistical parameters

For model performance and other comparison purposes, correlation coefficient (r), bias, root mean square error (rmse) and scatter index (S_i) were calculated based on the following relevant equations:

$$r = \frac{\sum_i((x_i - \overline{x})\,(y_i - \overline{y}))}{\sqrt{((\sum_i(x_i - \overline{x})^2)\,(\sum_i(y_i - \overline{y})^2))}} \quad \ldots (2)$$

$$Bias = \frac{1}{n}\sum_i(y_i - x_i) \quad \ldots (3)$$

$$rmse = \frac{1}{n}\sum_i(y_i - x_i)^2 \quad \ldots (4)$$

$$S_i = \frac{rmse}{\overline{x}} \quad \ldots (5)$$

where (x_i) and (y_i) represent same parameter observed and predicted values or values of different resolutions at the (i^{th}) time step of the record; length is represented by (n) and the bar ($^-$) denotes the average value of a certain parameter over time.

Results and Discussion

SWAN model was initially forced by GFS4_anl wind filed with the highest available temporal and spatial resolutions (THHD). As an example, Figure 3 shows forcing wind field (GFS4_anl) for March 18, 2010 at 18:00 hrs as well as SWAN-obtained significant wave height and peak wave period for the whole Red Sea. At that specific time, forcing winds reached their maximum speeds in the northern part of the Red sea with values exceeding 15 m/s in the upper north. Consequently, predicted significant wave heights reached their highest values at the northern part of the Red Sea with a maximum exceeding 4 m in the mid-north area. Predicted peak wave periods were also higher in the northern part of the Red Sea compared to the southern part.

Comparisons between observed and predicted parameters at buoy location are given in Figure 4 in the form of time series plots. The figure shows that despite the apparent disagreement between observed and model-obtained (GFS) forcing wind speeds at the buoy location, reasonable agreement is seen between observed and model-predicted wave heights. The comparison in terms of wave periods show less agreement between the observations and the model-predictions. Furthermore, comparisons between observed and predicted parameters at buoy location are made in the forms of scatter plots (Figure 5) and statistical parameters calculation (Table 3). Both scatter plots and statistics indicate that despite the apparently overestimating (Bias = 1.1643) and highly

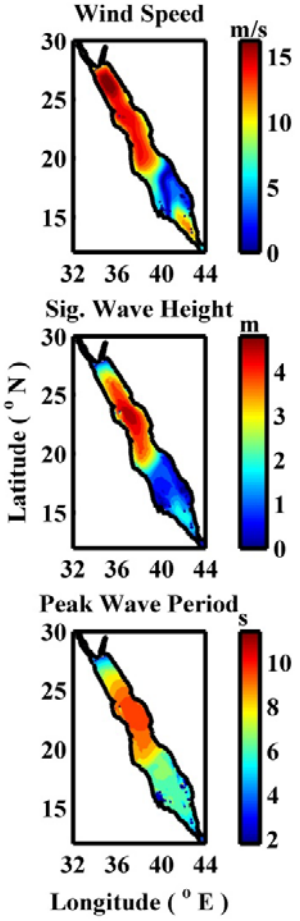

Fig. 3 — Forcing wind filed (top panel), model-obtained significant wave heights (middle panel) and model-obtained peak wave periods (bottom panel) for March 18, 2010 at 18:00 hrs.

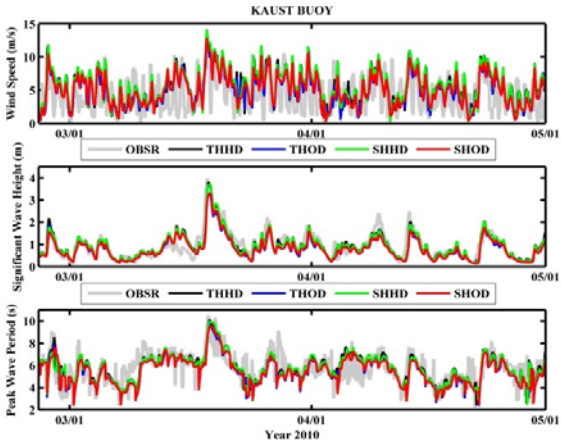

Fig. 4 — Time series plots at buoy location of observed vs. forcing wind speeds of different resolutions (top panel) and the corresponding observed vs. modeled significant wave heights (middle panel) and observed vs. modeled peak wave periods (bottom panel).

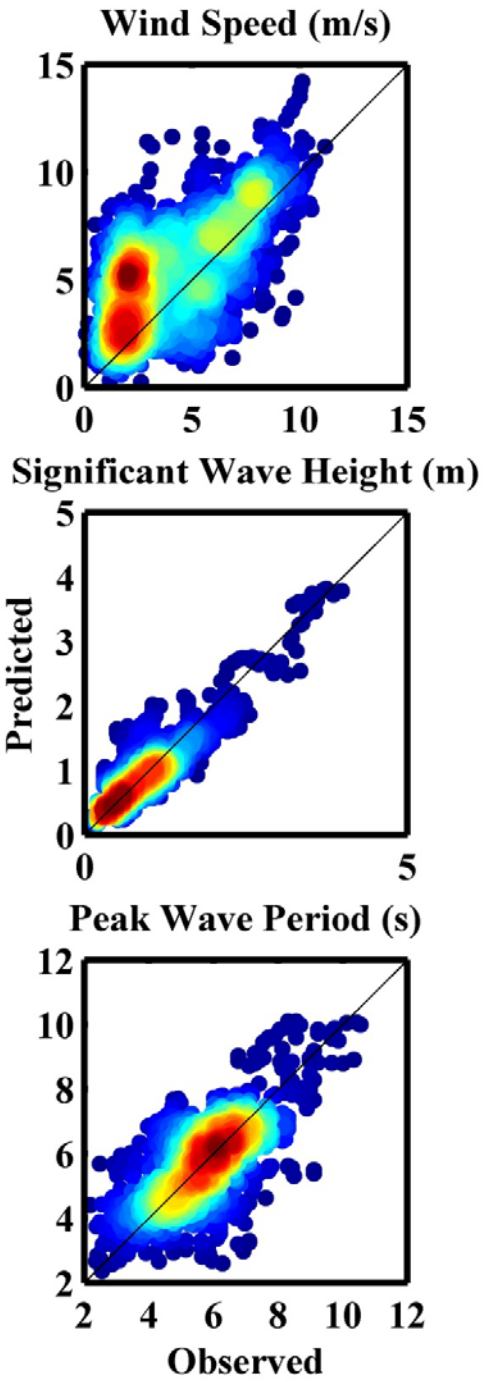

Fig. 5 — Scatter plots at buoy location of observed vs. forcing wind speeds of different resolutions (top panel) and the corresponding observed vs. modeled significant wave heights (middle panel) and observed vs. modeled peak wave periods (bottom panel). Color gradient indicates data points density variation from high (red) to low (blue).

scattered (S_i = 0.5494) forcing wind field, the model-predicted wave heights are showing reasonable agreement with the observed wave heights (Bias = 0.00003) and consequently a much lower scattering (S_i = 0.2751). Additionally, the relatively high correlation (r = 0.8894) between observed and predicted significant wave heights indicates that the wave height pattern is considerably reserved by the model. Statistical comparisons of observed and predicted peak wave periods show more agreement (Bias = 0.0264) and less scattering (S_i = 0.1772) than wind speeds, but less agreement and more scattering than significant wave heights. To a large extent, similar results were also obtained by the above-mentioned previous studies that attempted to simulate wave conditions in the Red Sea using SWAN model.

Three additional SWAN model runs were made with forcing wind fields of different temporal and/or spatial resolutions (THOD, SHHD and SHOD) which, according to Figures 4 and 6 and Table 3, have apparent disagreement (at buoy location) not only with observations but also among themselves. In the form of scatter plots, the left-side panels of Figure 6 show comparisons between the original (highest resolution) wind filed (THHD) and the three wind fields of different resolutions, while middle and right-side panels show the wave heights comparisons and the peak period comparisons, respectively. Table 3 includes statistical comparisons between different forcing wind fields and between the corresponding wave heights and between the corresponding peak periods. Figure 6 shows apparent underestimations of wind speeds at buoy location by both THOD and SHOD in comparison to THHD, while there is much less underestimation by SHHD. This can also be indicated from Table 3, which shows better agreement (Bias = 0.0680) between THHD and SHDD winds in comparison to that between THHD and THOD (Bias = - 0.5330) and between THHD and SHOD (Bias = - 0.4743) winds. Consequently, as shown in Figure 6 and Table 3, there are apparent underestimations in wave heights as well as wave periods by both THOD and SHOD in comparison to THHD, while there is no underestimation by SHHD. Such results indicate that forcing wind spatial resolution difference (0.5° vs. 1º) has more significant effect than the temporal resolution difference (3 hrs vs. 6 hrs) on the quality of wave model predictions. This finding is supported by the significantly lower scattering (S_i = 0.0716) between SHHD and THDD wave heights in comparison to more than two times higher scattering by both THOD (S_i = 0.1526) and SHOD (S_i = 0.1675)

Table 3 — Calculated statistical parameters for observed vs. modeled and modeled vs. modeled wind speeds, significant wave heights and peak wave periods.

		Wind Speed				Significant Wave Height				Peak Wave Period			
		THHD	THOD	SHHD	SHOD	THHD	THOD	SHHD	SHOD	THHD	THOD	SHHD	SHOD
OBSRV	r	0.6552	0.6450	0.6397	0.6226	0.8894	0.8870	0.8959	0.8956	0.6926	0.6960	0.6749	0.6973
	Bias	1.1643	0.6312	1.2323	0.6900	0.00003	-0.1219	-0.0065	-0.1263	0.0264	-0.2231	-0.0257	-0.2724
	rmse	2.3958	2.1299	2.4630	2.2038	0.2751	0.3055	0.2672	0.2979	1.0146	1.0157	1.0399	1.0290
	S_i	0.5494	0.4884	0.5648	0.5054	0.2930	0.3253	0.2846	0.3173	0.1772	0.1774	0.1816	0.1797
THHD	r		0.9876	0.9649	0.9538		0.9963	0.9926	0.9894		0.9674	0.9652	0.9528
	Bias		-0.5330	0.0680	-0.4743		-0.1220	-0.0065	-0.1263		-0.2495	-0.0522	-0.2988
	rmse		0.6962	0.6712	0.9053		0.1466	0.0675	0.1573		0.4063	0.3366	0.4869
	S_i		0.1260	0.1215	0.1639		0.1526	0.0716	0.1675		0.0706	0.0585	0.0846
THOD	r			0.9600	0.9678			0.9911	0.9937			0.9531	0.9668
	Bias			0.6010	0.0587			0.1154	-0.0044			0.1974	-0.0492
	rmse			0.9324	0.5820			0.1481	0.0569			0.4287	0.3176
	S_i			0.1868	0.1166			0.1812	0.0689			0.0779	0.0577
SHHD	r				0.9889				0.9970				0.9646
	Bias				-0.5423				-0.1198				-0.2466
	rmse				0.6894				0.1378				0.4132
	S_i				0.1233				0.1478				0.0725

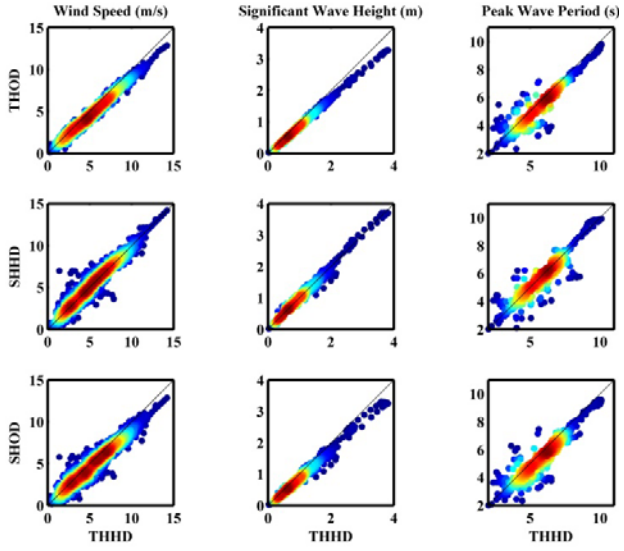

Fig. 6 — Scatter plots at buoy location of wind speed of highest resolution (THHD) vs. other wind speeds of different resolutions (left-side panels) and the corresponding model obtained wave heights (middle panels) and peak wave periods (right-side panels). Color gradient indicates data points density variation from high (red) to low (blue).

wave heights (Table 3). Similarly, in terms of wave period, Table 3 shows less scattering between SSHD and THHD (S_i = 0.0585) in comparison to higher scattering by both THOD (S_i = 0.0706) and SHOD (S_i = 0.0846). Additional statistical comparisons given in Table 3 also show that, in terms of wind speeds and consequently wave heights and peak wave periods, the root mean square errors are consistently higher in magnitude between similar parameters of different spatial resolutions. This also confirms that the forcing wind spatial resolution has more significant effect than the temporal resolution on the quality of the predictions of the SWAN-base Red Sea wave model.

Being a spectral model, SWAN also allowed to look at differences among the predicted wave spectra obtained using forcing winds of different resolutions. Although lacking observed wave spectra to compare with, comparisons were made in terms of the observed peak wave frequency (frequency of highest energy) which is the reciprocal of observed peak wave period. As an example, Figure 7 shows normalized wave spectra obtained with different spatial and temporal wind field resolutions. The figure is showing an agreement between observed peak wave frequency and the peak wave frequency of the model-predicted spectrum obtained using the highest spatial and temporal resolutions forcing wind field

(THHD). For all other predicted wave spectra obtained with forcing wind fields of different resolutions (THOD, SHHD and SHOD), computed peak wave frequencies were shifted toward higher frequencies range in comparison to observed peak wave frequency. Such results indicate wave model sensitivity to both temporal and spatial resolutions of the forcing wind fields. However, Figure 7 also shows some similarity between the spectra obtained with winds of similar spatial resolutions in comparison to those obtained with winds of similar temporal resolutions indicating that wave model is more sensitive to the spatial resolution of forcing wind fields. The 2-D wave spectral plots, given in Figure 8, show that the shifting apply not only to peak wave frequencies but also to peak wave directions (directions of highest energy). These results indicate that with changes in spatial and/or temporal resolution the forcing wind field will cause changes in the wave energy distribution over both frequency and directional domains. Such an effect will become even more important as the waves approach coastal areas where wave energy distribution significantly influences dissipation and transformation mechanisms. To investigate changes on energy distribution over the temporal domain due to use of forcing wind fields of different resolutions, spectral time series plots, given in Figure 9, were compared. The comparisons showed that the energy distributions pertaining to THHD and THOD have more agreement with each other and less agreement with SHHD and SHOD which in turn have more agreement with each other. This suggests that energy distribution over time is affected by the temporal difference in the wind filed resolution.

For the 20 ENVISAT tracks utilized, Figure 10 shows a comparison between along-track observed and the THHD wind speeds as well as the comparison between the along-track observed and model-predicted significant wave heights in the form of scatter plots, while Table 4 includes the corresponding statistical comparisons. Both Figure 10 and Table 4 show that despite the apparent underestimation by THHD forcing wind field (Bias = - 0.2444), the predicted wave heights show a slight overestimation (Bias = 0.0659). Although the corresponding errors for wind speeds (rmse = 1.4114) and wave heights (rmse = 0.3306) reflect big difference, the scatter indices were in the same order of magnitude with wave heights slightly more scattered. The comparisons between the along-track

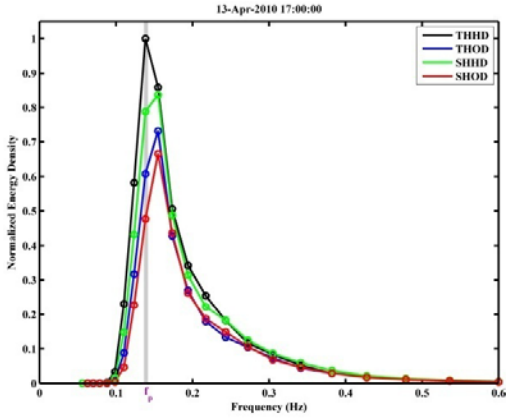

Fig. 7 — Normalized model-obtained 1D wave spectra (for Apr. 13, 2010 17:00) with forcing wind fields of different resolutions. Grey vertical straight line represents the peak wave frequency (f_p).

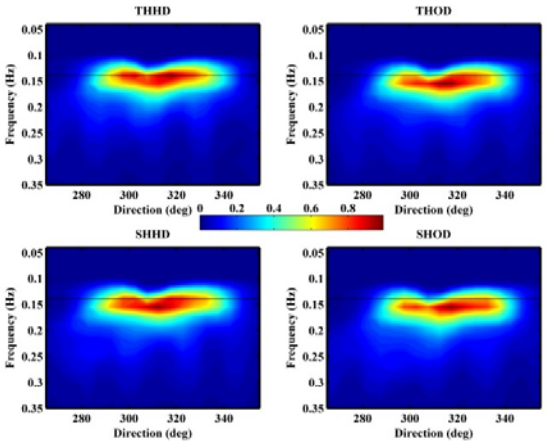

Fig. 8 — Normalized model-obtained 2D wave spectra (for Apr. 13, 2010 17:00) with forcing wind fields of different spatial and temporal resolutions. Black horizontal straight line represents the peak wave frequency (f_p).

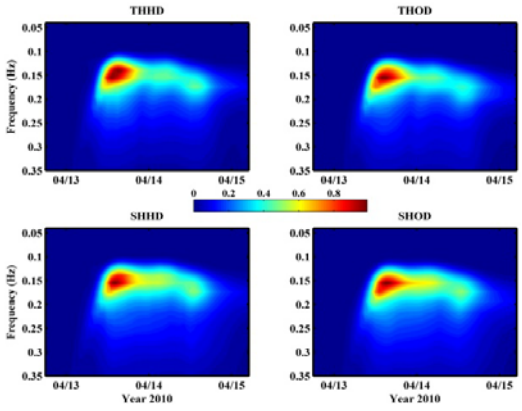

Fig. 9 — Time series plots of normalized model-obtained 1D spectra during two days in March 2010 with forcing wind fields of different resolutions.

Table 4 — Calculated statistical parameters for observed vs. modeled and modeled vs. modeled wind speeds and significant wave heights.

		Wind Speed				Significant Wave Height			
		THHD	THOD	SHHD	SHOD	THHD	THOD	SHHD	SHOD
OBSRV	r	0.8092	0.7895	0.8258	0.8085	0.7677	0.7566	0.7527	0.7400
	Bias	-0.2444	-0.6543	-0.0612	-0.4805	0.0659	-0.0876	0.0442	-0.1060
	rmse	1.4114	1.5193	1.3063	1.3705	0.3306	0.3351	0.3344	0.3491
	S_i	0.2153	0.2317	0.1993	0.2091	0.2834	0.2882	0.2876	0.3002
THHD	r		0.9827	0.9812	0.9691		0.9845	0.9936	0.9742
	Bias		-0.4098	0.1832	-0.2360		-0.1536	-0.0217	-0.1719
	rmse		0.6156	0.4905	0.6514		0.1797	0.0560	0.2070
	S_i		0.0975	0.0777	0.1032		0.1462	0.0456	0.1684
THOD	r			0.9599	0.9831			0.9811	0.9925
	Bias			0.5931	0.1738			0.1319	-0.0184
	rmse			0.9324	0.5820			0.1608	0.0517
	S_i			0.1486	0.0738			0.1495	0.0481
SHHD	r				0.9809				0.9836
	Bias				-0.4193				-0.1503
	rmse				0.6317				0.1761
	S_i				0.0973				0.1459

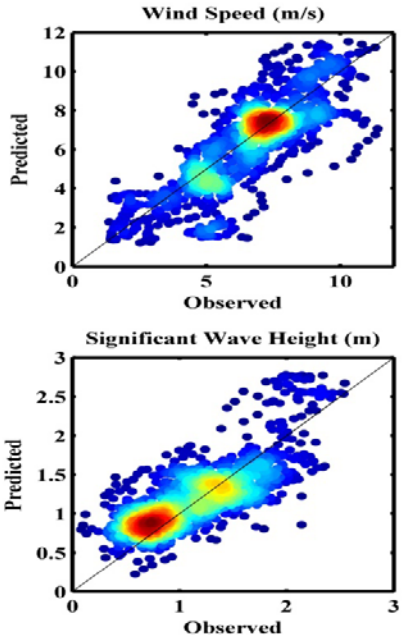

Fig. 10 — Scatter plots of along-track observed vs. forcing wind speeds of different resolutions (top panel) and the corresponding observed vs. modeled significant wave heights (bottom panel). Color gradient indicates data points density variation from high (red) to low (blue).

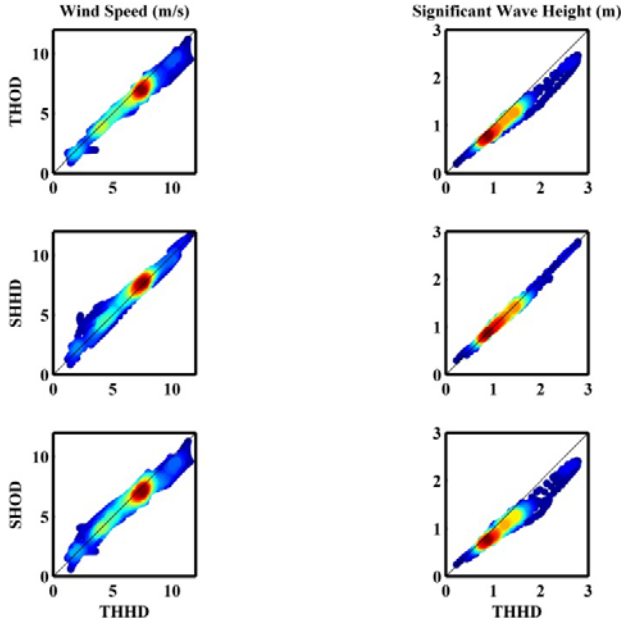

Fig. 11 — Scatter plots of along-track wind speed of highest resolution (THHD) vs. other along-track wind speeds of different resolutions (left-side panels) and the corresponding model obtained wave heights (right-side panels). Color gradient indicates data points density variation from high (red) to low (blue).

THHD and other wind fields (THOD, SHHD and SHOD) as well as the corresponding along-track predicted wave heights are given in the form of scatter plots (Fig. 11) and statistics (Table 4). Figure 11

shows the underestimation by both THOD and SHOD in comparison to SHHD in terms of both wind speeds and wave heights. Table 4 shows that in terms of along-track predicted wave heights the bias obtained between THHD and SHHD (-0.0217) was much smaller in magnitude than the biases obtained between THHD and THOD (-0.1536) and between THHD and SHOD (-0.1719). Additional statistical comparisons given in Table 4 also show that, in terms of wind speeds and consequently predicted wave heights, root mean square errors; and scatter indices are consistently higher in magnitude between similar parameters of different spatial resolutions. Such results indicate that the forcing wind spatial resolution has more significant effect than the temporal resolution on the quality of the predictions of the SWAN-based Red Sea wave model.

Conclusion

The sensitivity of a SWAN-based Red Sea wave model to forcing wind field spatial and temporal resolutions has been fully investigated. The parametric comparisons at buoy location and along satellite tracks showed better agreements between similar predicted parameters of similar spatial resolutions, indicating that the wave model is much more sensitive to the spatial resolution of the forcing wind field. However, the spectral comparisons among the predicted 1-D and 2-D spectra showed slight shifts in energy distribution over frequency, directional and temporal domains, suggesting that the spectral wave model is also sensitive to temporal resolution of the forcing wind field.

Acknowledgement

The authors are thankful to King Abdullah University for Science and Technology (KAUST) and for National Data Buoy Center (NDBC) for making available the data collected by Met/Ocean buoy (NDBC: 23020). Thanks are also due to National Oceanic and Atmospheric Administration (NOAA) for making available Global Forecasting System (GFS) predicted wind filed, to General Bathymetric Chart of the Oceans (GEBCO) for making available the bathymetric data and to Technical University of Delft for providing the ENVISAT wind and wave observations.

References

1 Ponce de León, S. & Ocampo-Torres, F., Sensitivity of a wave model to wind variability, *J. Geophys. Res*., 103:C2 (1998) 3179-3201.

2 Signell R., Carniel, S., Cavaleri, L., Chiggiato, J., Doyle, J., Pullen, J. & Scalvo, M., Assessment of wind quality for oceanographic modelling in semi-enclosed basins, *J. Marine Syst.*, 52 (2005) 217-233.

3 Feng, H., Vandemark, D., Quilfen, Y., Chapron, B. & Beckley, B., Assessment of wind forcing on global wind-wave model using the TOPEX altimeter, *Ocean Eng.*, 33:11-12 (2006) 1431-1461.

4 Ponce de León, S. & Soares, C., Sensitivity of wave model predictions to wind fields in the Western Mediterranean Sea, *Coast. Eng.*, 55 (2008), 929-929.

5 Rusu, L., Bernardino, M. & Soares C., Influence of the wind fields on the accuracy of numerical wave modelling in offshore locations, Presented at the *International Conference on Offshore Mechanics and Arctic Engineering*, Estoril, Portugal, 2008.

6 Rusu, L., Bernardino, M. & Soares C., Influence of wind resolution on the prediction of waves generated in an estuary, *J. Coastal Res.*, SI:56 (2009) 1419-1423.

7 Dominguez, M., *Coastal Wave Storms Observations and simulatioms in the NW Mediterranean*, Master Thesis, Universtat Politecnica de Catalunya (UPC), Spain, 2009.

8 Akpinar, A., Van Vledder G.Ph., Komurcu, M.I. & Ozger, M., Evaluation of the numerical wave model (SWAN) for wave simulation in the Black Sea, *Cont. Shelf Res.*, 50-51 (2012) 80-89.

9 Appendini, C., Torres-Freyermuth, A., Oropeza, F., Salles, P., Lopez, E. & Mendoza, T., Wave modeling performance in the Gulf of Mexico and Western Caribbean: wind reanalysis assessments, *Appl. Ocean Res.*, 39 (2013) 20-30.

10 Akpinar, A. & Ponce de León, S., An assessment of wind re-analyses in the modelling of an extreme sea state in the Black Sea, *Dynam. Atmos. Ocean.*, 73 (2016) 61-75.

11 Siadatmousavi, S., Jose, F. & Miot da Silva, G., Sensitivity of a third generation wave model to wind and boundary condition sources and model physics: a case study from the South Atlantic Ocean off Brazil coast, *Comput. Geosci.*, 90:B (2016) 57-65.

12 Van Vledder, G.Ph. & Akpinar, A., Wave model predictions in the Black Sea: sensitivity to wind fields, *Appl. Ocean Res.*, 53 (2015) 161-178.

13 Morcos, S., Physical and chemical oceanography of the Red Sea, *Oceanogr. Mar. Biol.*, 8 (1970) 73-202.

14 Patzert, W., Wind induced reversal in the Red Sea circulation, *Deep-Sea Res.*, 21 (1974) 109-121.

15 Edwards, A., *Red Sea*, (Pergamon Press, Oxford) 1987, pp. 441.

16 Al-Barakati, A., Residual currents in coastal waters near Jeddah desalination plants, Red Sea, *J. King Abd. Uni. Mar. Sci.*, 20 (2004) 49-58.

17 Zubier, K.M., Aboulnaja, Y.O. & Al-Subhi, A.M., Development of an operational wave prediction system for the Red Sea: experimental phase, Presented at the *Offshore Arabia Conference*, Dubai, United Arab Emirates, 2009.

18 Gharbi, S., *Numerical wave simulation in the Red Sea*, Master Thesis, King Abdulazizi University, Saudi Arabia, 2012.

19 Fery, N., Bruss, G., Al-Subhi, A. & Mayerle, R., Numerical study of wind generated waves in the Red Sea, Presented at the *International Conference on the Application of Physical Modeling to Port and Coastal Protection*, Ghent, Belgium, 2012.

20 Ralston, D., Jiang, H. & Farrar, J., Waves in the Red Sea: response to monsoonal and mountain gap winds, *Cont. Shelf Res.*, 65 (2013) 1-13.

21 Langodan, S., Cavaleri, L., Viswanadhapalli, Y. & Hoteit, I., The Red Sea: a natural laboratory for wind and wave modeling, *J. Phys. Oceanogr.*, 144:12 (2014) 3139-3159.

22 Fery, N., Al-Subhi, A., Zubier, K. & Bruss, G., Evaluation of the sea state near Jeddah based on recent observations and model results, *J. Oper. Oceanogr.*, 8:1 (2015) 1-10.

23 Langodan, S., Cavaleri, L., Viswanadhapalli, Y. & Hoteit, I., Wind-wave source function in opposing seas, *J. Geophys. Res.-Oceans*, 120 (2015) 3751-6768.

24 Aboobacker, V.M., Shanas, P.R., Alsaafani, M.A. & Albarakati, A.M., Wave energy resource assessment for Red Sea, *Renew. Energ.*, 114:A (2016) 46-58.

25 Langodan, S., Viswanadhapalli, Y., Dasari, H. P., Kino, O. & Hoteit, I., A high-resolution assessment of wind and wave energy potentials in the Red Sea, *Appl. Energ.*, 181 (2016) 244-255.

26 Langodan, S., Viswanadhapalli, Y. & Hoteit, I., The impact of atmospheric Data assimilation on wave simulations in the Red Sea, *Ocean Eng.*, 116 (2016) 200-215.

27 Shanas, P.R., Aboobacker, V.M., Albarakati A.M. & Zubier, K.M., Superimposed wind-waves in the Red Sea, *Ocean Eng.*, 138 (2017) 9-22.

28 Langodan, S., Cavaleri, L., Pomaro, A., Viswanadhapalli, Y., Bertotti, L. & Hoteit, I., The climatology of the Red Sea – part 2: the waves, *Int. J. Climatol.*, 37 (2017) 4518-4528.

29 Ris, R., *Spectral modeling of wind waves in coastal areas*, Ph.D. Dissertation, Delft University of Technology, Netherlands, 1997.

30 Booij, N., Ris, R. & Holthuijsen, L., A third generation wave model for coastal regions; part i: model description and validation, *J. Geophys. Res*., 104:C4 (1999) 7649-7666.

31 Ris, R., Booij, N. & Holthuijsen, L., A third generation wave model for coastal regions; part ii: verification, *J. Geophys. Res*., 104(C4) (1999)., 7667-7681.

32 The SWAN team, *SWAN user manual: SWAN cycle iii - version 41.10*, Delft University of Technology, Netherlands, 2016.

33 Dykes, J.D., Hsu, L.Y. & Rogers, E.W., *The development of an operational SWAN model for NGLI*, (Proceedings of the Oceans 2002 MTS/IEEE Conference, Biloxi, Mississippi), (2002) 859-866.

34 Zubier, K., *Numerical wave simulations on different oceanic scales*, Ph.D. Dissertation, University of Maine, USA, 2002.

35 Zubier, K., Panchang, V. & Demirbilek, Z., Simulation of waves at Duck (North Carolina) using two numerical models, Coast. Eng. J., 45:3 (2003) 439-469.

36 Moeini, M.H. & Etemad-Shahidi A.E., Wave parameter hindcasting in a lake using the SWAN model, *Civil Eng.*, 16:2 (2009) 156-164.

37 Moeini, M., Etemad-Shahidi, A. & Chegini, V., Wave modeling and extreme value analysis off the northern coast of the Persian Gulf, *Appl. Ocean Res.*, 32 (2010) 209–218.

38 Arkhipkin, V.S., Gippius, F.N., Koltermann, K.P. & Surkova, G.V., Wind waves in the Black Sea: results of a hindcast study, *Nat. Hazard. Earth Sys.*, 14 (2014) 2883–2897.

39 Cooper, A.H. & Mulligan, R.P., Application of a spectral wave model to assess breakwater configurations at a small craft harbour on Lake Ontario, *J. Mar. Sci. Eng.*, 4:46 (2016) 1-11.

40 Liau, Y. & Kaihatu, J.M., Numerical investigation of wind waves in the Persian Gulf: bathymetry effects, *J. Atmos. Ocean. Tech.*, 33 (2016)., 17-31.

41 Mao, M., van der Westhuysen, A.J., Xia, M., Schwab, D.J. & Chawla, A., Modeling wind waves from deep to shallow waters in Lake Michigan using unstructured SWAN, *J. Geophys. Res.-Oceans*, 121 (2016) 3836–3865.

42 Myslenkov, S. & Chernyshova, A., Comparing wave heights simulated in the Black Sea by the SWAN model with satellite data and direct wave measurements, *Russ. J. Earth Sci.*, 16:5 (2016) 1-12.